A monopolar vortex encounters an isolated topographic feature on a β-plane

J.H.G.M. van Geffen [*], P.A. Davies

Department of Civil Engineering, University of Dundee, Dundee DD1 4HN, UK

Abstract

A two-dimensional (2D) numerical model is used to investigate the possible effects of a cosine-shaped, circularly symmetric seamount on the motion of a monopolar vortex on a β-plane. The monopole moves to the northwest due to the β-effect and encounters the seamount from the southeast. The lateral dimension of the topographic feature is varied between one and four times that of the monopole and the seamount is located at latitudes between far south and far north of the equator. For comparable topographic and vortex scales, the monopole's trajectory differs somewhat from its trajectory in the absence of any bottom topography, the difference being bigger for mountains further away from the equator. Large seamounts in the southern hemisphere can deflect the monopole more towards the north or they can rebound the monopole back to the southeast, thus forming a barrier for the vortex. Large seamounts in the northern hemisphere deform the monopole significantly, leading to complicated trajectories after the vortex has crossed the topography, or to trapping (permanently or temporarily) by the topography. If it is trapped, the monopole circles around the top of the mountain, while performing small loops, and it is eventually destroyed by the topography-induced vorticity. © 2000 Elsevier Science B.V. All rights reserved.

Keywords: Vortex; Topographic feature; β-plane

1. Introduction

Vortices are common phenomena under many geophysical circumstances. In the Earth's oceans, for example, Meddies, Gulf Stream eddies and anticyclones, Agulhas

---

[*] Corresponding author. Royal Netherlands Meteorological Institute, P.O. Box 201, 3730 AE De Bilt, The Netherlands

eddies, etc. have been observed (see, e.g., Richardson, 1993a,b; Bower et al., 1995; Kamenkovich et al., 1996; Bograd et al., 1997). These vortices move through the oceans due to a combination of the ambient flow and the latitudinal (y) variation of the Coriolis acceleration (the so-called β-effect). On their way through the ocean, these eddies encounter topographic features at the ocean floor. It is known that such an encounter affects the eddy's trajectory. This can lead to large deformations of the eddy, or even to its destruction (e.g., Richardson, 1993a,b; Shapiro et al., 1995), as a consequence of which the contents of the eddy may be released in the ocean. Though the background of the study presented here is a vortex that encounters a topography in oceans, similar processes can be of importance for the evolution of large-scale vortices in the atmosphere (for reviews see, e.g., Bengtsson and Lighthill, 1982; Hopfinger and Van Heijst, 1993).

Since oceanic vortices are thought to play an important role in the transport of water properties (such as salt, heat, momentum and pollutants), it is of importance to understand the basic mechanisms of what happens if a vortex encounters bottom topography. In that light, the present numerical study considers the effect of a circular mountain on the motion and evolution of a monopolar vortex, as a model for what could happen to an oceanic vortex. In Section 3.1, comparisons are made between the key controlling parameters of the model and the oceanic eddies under consideration, in order to establish the relevance of the results to oceanic processes. The monopole in the simulations is cyclonic (anti-cyclonic) in the northern (southern) hemisphere and it moves to the northwest due to the β-effect (see, e.g., Van Heijst, 1994). Carnevale et al. (1991) have shown with laboratory and numerical experiments that in the northern hemisphere a cyclonic monopole, when placed on a hill, climbs to the top of the hill in an anti-cyclonic spiral. The reason for this is that the β-effect is dynamically equivalent to a sloping bottom boundary, with north towards shallow fluid depth (Van Heijst, 1994); hence, for a hill the local topography-induced northwest is uphill and to the left.

In their experiments, Carnevale et al. (1991) used a monopole that was much smaller in lateral size than the topography and the monopole was released on the topography. In the present study, however, the monopole is initialised at a position to the southeast of the seamount. The radius of this mountain (R) is varied from the same size as to four times that of the monopole (a). The latter moves due to the β-effect, represented by βy in the Coriolis parameter $f = f_0 + \beta y$, with y as the local north coordinate. Carnevale et al. (1991) used two positive values of f_0, representing a topography located at two latitudes in the northern hemisphere. In the case study numerical simulations discussed below, β is kept constant at 0.3 (dimensionless units) and f_0 is varied from -5 to $+5$, thus representing encounters taking place between far south and far north of the equator (for $f_0 = 0$, the mountain is at the equator). Such extreme cases capture the essential features and ranges of the possible effects of a seamount on a vortex.

A range of numerical experiments in which a dipolar vortex (a modon) encounters a topography (ridge, hill, random or other) was presented by Carnevale et al. (1988). They observed in some cases effects of shedding of vorticity from the topography during the approach of the vortex similar to the effects discussed below. Carnevale et al. (1988) observed these effects, for instance, when the modon breaks up if it encounters a hill, in which case the positive vortex is seen to move uphill, where it can remain trapped; the

negative vortex, meanwhile, moves away from the hill, together with positive vorticity generated by the flow across the hill. Modon breakup occurs on a hill with a horizontal scale similar to or somewhat less than that of the modon. In the present study, the monopole is of the same size as or smaller than the mountain.

The numerical model used is the same as that of Van Geffen and Davies (1999a; b): a one-layer two-dimensional (2D) barotropic model with rigid-lid approximation, with bottom topography suitably incorporated. Section 2.3 reviews the main assumptions and approximations of the model in relation with oceanic vortices such as those mentioned above.

Van Geffen and Davies (1999a; b) showed that when a monopole encounters a 2D topographic ridge, the height and width of the ridge and the value of f_0 (or, equivalently, the north–south position of the encounter) determine the evolution of the monopole: the vortex can cross the ridge, be trapped on the ridge and decay there, be destroyed on the ridge by strong vorticity gradients, or be rebounded by the ridge without reaching the foot of the ridge. The above studies have illustrated the practical difficulties in categorising flows corresponding to the many combinations of the free parameters of the problem. Accordingly, in the present study, the most profitable approach is considered to be that of the case study, for fixed values of some of the controlling parameters. The height of the cosine-shaped, circularly symmetric seamount, for example, is kept fixed at $h_{max} = 0.4$, relative to the fluid depth away from the topography, whereas its radius R is varied. Varied is also the value of f_0 in the Coriolis parameter, as mentioned above. All other model parameters remain unchanged.

The remainder of the paper is organised as follows. The model and some computational aspects are given in the next section. Section 3 presents the results of the simulation and some concluding remarks are formulated in the Section 4.

2. Description of the model

This section describes in brief the model equations and some computational aspects — for more details, the reader is referred to Van Geffen and Davies (1999a) — and it introduces the monopole and the isolated seamount topography used in the simulations. The section ends with a discussion of some of the assumptions made in the model.

2.1. The numerical method

The numerical model is based on the assumption that the motions in the fluid are (quasi-) 2D and bounded above by a ridig lid, such that the topography-induced vertical motion w is much smaller than the horizontal motions u, v, with $\boldsymbol{v} = (u, v, w)$ the relative velocity of the flow in a Cartesian coordinate system. The relative vorticity ω of this flow is then given by $\boldsymbol{\omega} = \omega \boldsymbol{k} = \nabla \times \boldsymbol{v}$, with $\boldsymbol{k}$ the unit normal vector in the vertical (z) direction. The evolution in time of ω is described by the 2D Navier–Stokes equation in the vorticity–streamfunction formulation:

$$\frac{\partial \omega}{\partial t} + J\left(\omega_p, \psi_p\right) = \nu \nabla^2 \omega, \tag{1}$$

where ν is the kinematic viscosity, J the Jacobian operator (describing the non-linear advection effects) and ψ_p a streamfunction defined by:

$$\begin{cases} Hu = \partial\psi_p/\partial y \\ Hv = -\partial\psi_p/\partial x \end{cases} \text{or} \ \ H\boldsymbol{v} = \nabla \times \boldsymbol{k}\psi_p = \nabla\psi_p \times \boldsymbol{k}. \tag{2}$$

Some authors (e.g., Grimshaw et al., 1994) denote ψ_p as the ''mass transport streamfunction''. Van Geffen and Davies (1999a) have preferred to denote this quantity as the ''potential streamfunction'' because of its clear connection with the potential vorticity ω_p; the two terms are completely equivalent. In Eq. (1), the potential vorticity is given by:

$$\omega_p = \frac{\omega + f}{H}, \tag{3}$$

where f is the Coriolis parameter, describing the latitudinal (y) variation of the vertical component of the Earth's angular velocity. In the so-called β-plane approximation used in the present paper, the Coriolis parameter with respect to a reference latitude is given by (e.g., Van Heijst, 1994):

$$f = f_0 + \beta y + \mathcal{O}(y^2), \tag{4}$$

with y as the local north coordinate.

The relation between vorticity and streamfunction is given by what can be denoted the modified Poisson equation:

$$H\omega = -\nabla^2\psi_p + \frac{1}{H}(\nabla H \cdot \nabla\psi_p), \tag{5}$$

which reduces to the regular Poisson equation $\omega = -\nabla^2\psi$ for a uniform fluid depth (with ψ as the regular streamfunction).

If Eq. (1) is made dimensionless using a typical length scale L_0 and a typical time scale T_0, the familiar Reynolds number Re appears: $Re = L_0^2/T_0\nu$. In what follows, these typical scales are set equal to unity, so that the Reynolds number, in effect, is $Re = 1/\nu$, and all quantities are given in dimensionless units (see Van Geffen and Davies, 1999a). This implies that a vortex with a translation velocity of 2, say, travels 2 length units in 1 time unit. What is chosen for the parameters in the simulations and what that means for the length and time scales involved is discussed in Section 3.1. The default fluid depth, away from any topography, is scaled to $H = 1$, a scaling that is independent of the horizontal scale L_0.

Eqs. (1) and (5) form the set of equations solved by the numerical method for given $H = H(x, y)$, f_0 and β, starting from an initial vorticity distribution $\omega(x, y, t = 0)$.

The equations are solved with a finite difference method on a rectangular grid in a rectangular x, y-domain. The time evolution in Eq. (1) is computed with an explicit third-order Runge–Kutta scheme, the viscous term $\nu\nabla^2\omega$ with a Crank–Nicolson scheme and the nonlinear term $J(\omega_p, \psi_p)$ with the Arakawa scheme. The use of the

Arakawa scheme (Arakawa, 1966) guarantees, on the one hand, that in the inviscid case energy, entropy and skew symmetry are conserved, and, on the other hand, that the computations have a high degree of stability. Eq. (5) is solved with a multigrid method by a routine from the NAG Library, which limits the number of grid cells to 2^n ($n = 1,2,3, \dots$) in either direction.

The possible effects of the boundaries of the domain are minimised by using a stress-free condition on the boundaries (which means that the boundary is a streamline along which the fluid can flow freely, without being able to pass through the boundary) and by using a domain that is much larger (see below) than the diameter of the monopolar vortex that is used.

2.2. The monopole, the domain and the seamount

The vortex is represented at $T = 0$ by a monopolar vortex of Bessel type, with a vorticity distribution given by:

$$
\omega = \begin{cases} \dfrac{(ka)\Gamma}{2\pi a^2 J_1(ka)} J_0(kr), & r \leq a \\ 0, & r \geq a, \end{cases}
\tag{6}
$$

where r is the radial distance to the centre of the vortex, a its radius, and Γ its strength or circulation. J_0 and J_1 are Bessel functions of the first kind and $ka \approx 2.4048$ is the first non-zero root of J_0. The maximum of vorticity is located at the centre of the monopole, where J_0 equals unity. This axisymmetric vortex is an exact, stationary solution of the inviscid vorticity equation for a constant Coriolis parameter and in the absence of any topography in an infinite domain, satisfying the linear relationship $\omega = k^2\psi$. The outcome of the encounter of the topography by the monopole is therefore not influenced by possible instabilities in the vortex itself.

The simulations are performed with a monopole with $a = 0.5$ and $\Gamma = +4$, hence, the monopole is cyclonic (anti-cyclonic) in the northern (southern) hemisphere. The monopole is initialised at $(x_0, y_0) = (+3, -3)$ in a 20×20 domain centred at the origin.

The influence of the size of the domain on the monopole's evolution has been subject to a sensitivity study (see Van Geffen and Davies, 1999a) and a 20×20 domain has been found to be sufficiently large to neglect possible effects of the boundaries of the domain. In Van Geffen and Davies (1999a), the topography was a ridge extending to the boundaries, whereas in the present study the topography is a seamount of small size, small compared with the size of the domain, hence the effect of the boundaries of the 20×20 domain on the monopole's evolution can be neglected in the present study as well.

Due to the β-effect the monopole will move to the northwest (see, e.g., Van Heijst, 1994). The trajectory the monopole follows is not a straight line but one containing bends and kinks in it (see, for instance, the solid line in Fig. 1) because, as the monopole moves, it leaves behind vorticity in the form of Rossby waves. The monopole itself interacts subsequently with this β-induced vorticity (by some authors named beta-gyres).

In the absence of any topography, the monopole passes then roughly through the origin of the domain. And when $\beta = 0.3$, as in the present study, the monopole completes its trajection at about $(-3, +3)$ at $T = 50$ (the end time of most simulations), as shown by Van Geffen and Davies (1999a). For larger (smaller) β-values, the monopole decays faster (slower) due to the loss of vorticity as Rossby waves and the monopole does not end up roughly symmetric in the origin with respect to its starting point $(+3, -3)$. (Other combinations of Γ and β could, of course, result in a similar ''symmetry''; in that sense the choice $\Gamma = +4$ and $\beta = 0.3$ is somewhat arbitrary.)

On its way to the northwest, the monopole encounters an isolated, circularly symmetric, cosine-shaped mountain centred at the origin, its height h being given by:

$$h = \begin{cases} h_{\text{max}}\cos(r\pi/2R), & r \leq R \\ 0, & r \geq R, \end{cases} \tag{7}$$

The maximum height h_{max} of the topography is fixed at 0.4, which is about the largest value allowed within the assumption of 2D motions made for the model (the default fluid depth H being 1). The radius R of the mountain is varied between 0.5 and 2, i.e. between a and $4a$.

2.3. Review of the main model assumptions

Before presenting the results of the simulations, it is useful to review the assumptions made in the model and the appropriateness or otherwise of these approximations for the types of oceanic vortices mentioned in Section 1.

A key element of the model is the restriction to quasi-2D motions, such that $w \ll u$, v. Such a condition may be expressed (Pedlosky, 1987) in the form $w/U \ll h_{\text{max}}/L_{\text{s}}$, where U is a typical horizontal velocity and L_{s} is a horizontal scale dimension of the seamount. The right hand side of this inequality condition can be expressed as $(h_{\text{max}}/H)(H/L_{\text{s}})$, with the values of (H/L_{s}) and (h_{max}/H) being much less than unity and order unity, respectively, for the isolated abyssal seamounts of interest here. For example, for Fieberling (Eriksen, 1991; Goldner and Chapman, 1997), Ampère (Kunze and Sanford, 1993) and Irving (Shapiro et al., 1995) seamounts, the values of $(h_{\text{max}}/L_{\text{s}})$ are typically 0.07, 0.03 and 0.02, so that the 2D assumption $w/U \ll 1$ is easily satisfied for the flows in question.

The model also makes use of the β-plane assumption, with the dual implication in the model that (i) the β-effect is dynamically important in determining the behaviour of the vortex as it approaches and encounters the topographic disturbance and (ii) the $\mathcal{O}(y^2)$ term in Eq. (4) may be neglected. With regard to the latter constraint, it is easily shown that Eq. (4) can be written as:

$$f = (2\Omega_{\text{e}}\sin\phi_0) + (2\Omega_{\text{e}}\cos\phi_0/R_{\text{e}})y + (\Omega_{\text{e}}\sin\phi_0/R_{\text{e}}^2)y^2 + \ldots \tag{8}$$

with Ω_{e} as the rotation rate and R_{e} as the radius of the Earth:

$$\Omega_{\text{e}} = 7.27 \times 10^{-5}\,\text{s}^{-1}, \quad R_{\text{e}} = 6360\,\text{km} \tag{9}$$

and ϕ_0 as a reference latitude. For a typical oceanic eddy flow domain of 1000 km in horizontal extent (see, for example, Kamenkovich et al., 1996) and a vortex centred at a latitude of 30°, the second and third terms on the right hand side of Eq. (8) have values of 0.28 f_0 and 0.02 f_0, respectively. In the light of the earlier comments, such values confirm the validity of the β-plane approximation for the oceanic eddies under consideration here.

The ridig lid approximation adopted in the model is valid for baroclinic oceanic eddies when surface displacements are negligible compared with interface displacements (Gill, 1982). For the cases (e.g., Shapiro et al., 1995; Kamenkovich et al., 1996) in which field observations are available, the ratio of surface to interface displacements is typically much less than 10^{-2}.

It should be noted at this stage that the intention of the present paper is to report model results that hold generic interest (see also Carnevale et al., 1988; Van Heijst, 1994) for an understanding of idealised vortex–topography encounters in the oceans and atmosphere. Accordingly, the model configuration, though matching the oceanic conditions discussed above, contains drastic simplifications that obviate direct comparisons with specific oceanic eddies and eddy systems. One such simplification, for example, is the restriction to cases for which the full water column is homogeneous; such a configuration differs from that found with many relevant oceanic cases (such as meddies, for example) where buoyancy effects associated with the density difference between the eddy and its surrounding waters are dynamically significant. (In this regard, it is noted that Kamenkovich et al. (1996) have shown in their models of the Agulhas eddies that the behaviour of eddies approaching a submarine ridge may be quite different for baroclinic and barotropic cases.)

3. Results of the simulations

In the simulations of the encounter of topography (given by Eq. (7)) by monopole (given by Eq. (6)) described in this section, the radius R of the seamount and the value of the Coriolis constant f_0 are varied; all other parameters are kept constant.

3.1. The parameters in the simulations

For $f_0 = 0$ the equator is at $y_{eq} = 0$, i.e. it passes through the centre of the seamount. Varying f_0 is, as can be seen from the formulation in Eq. (4), equivalent to an encounter taking place north ($f_0 > 0$) or south ($f_0 < 0$) of the equator, the location of the equator being given by:

$$y_{eq} = -f_0/\beta, \tag{10}$$

where $\beta = 0.3$ is used for this study. For the motion of the monopole in the absence of topography, the value of the constant f_0 is unimportant, as can be seen from Eq. (1): the Coriolis parameter f only appears in the derivatives of the Jacobian operator. If the fluid depth H is a function of the position, however, the value of f_0 influences the evolution of the monopole and it is varied in the present study between $f_0 = -5$ and $f_0 = +5$.

The trajectory of the monopole is followed by a tracer initially placed at the centre of the monopole, where the maximum of vorticity ω_{max} is located. In most simulations the tracer remains at ω_{max}. Only when the interaction with the topography-induced vorticity introduces strong deformations of the vortex is the location of ω_{max} displaced from the tracer (in these cases, ω_{max} is located near one of the boundaries of the domain, or at or near the topography), even if there is still a clear vortex to be seen.

The 20×20 domain is divided in 256×256 grid cells (note that only a part of this domain is shown in the graphs), and values $\Delta t = 0.05$, $\beta = 0.3$ and $Re = 1000$ are used for all simulations presented here. The monopole is initialised at $(+3, -3)$ with $a = 0.5$ and $\Gamma = 4.0$. All runs end at $T = 50$, except for the cases with positive f_0 and $R > 1.0$ (Section 3.4) which end at $T = 100$.

The choice of the parameters a and Γ for the monopole and f_0 and β for the Coriolis parameter actually determine the length scale L_0 and the time scale T_0 used in the definition of the Reynolds number (Section 2.1). The size of the vortex is a natural length scale in the problem at hand. Denoting dimensional variables with an asterisk, this means that $L_0 = 2a^*$. Since f_0 is varied, β can be used for the time scale: $T_0 = \beta/(2a^*)\beta^*$, with by choice $\beta = 0.3$ here. (Alternatively, the choice for Γ could be used: $T_0 = \Gamma(2a^*)^2/\Gamma^*$, but using β seems more appropriate.)

The range of f_0-values then determines a range of corresponding latitudes for terrestrial phenomena once a value for a^* has been chosen. This follows from the definitions of f_0 and β in Eq. (8):

$$f_0^* = f_0/T_0 = 2\Omega_e \sin\phi_0, \quad \beta^* = \beta/L_0 T_0 = 2\Omega_e \cos\phi_0/R_e, \tag{11}$$

where the reference latitude ϕ_0 is obviously the latitude of the line $y = 0$ in the simulations. Combining the two equations in Eq. (11) gives:

$$f_0 = f_0(\phi_0) = \frac{\beta}{2a^*}\frac{f_0^*}{\beta^*} = \frac{\beta}{2a^*} \cdot R_e \cdot \tan\phi_0. \tag{12}$$

For an oceanic vortex with $L_0 = 2a^* = 10^5$ m (a typical size for e.g., a meddy; Richardson, 1993a) and $\beta = 0.3$, it follows that for, say, $\phi_0 = 15°N$: $f_0 = 5.11$, with the equator at $y_{eq} = -f_0/\beta = -17.04$ and time scale $T_0 = 1.36 \times 10^5$ s = 37.7 h. Similarly, $f_0(\phi_0 = 10°N) = 3.36$ and $f_0(\phi_0 = 5°N) = 1.67$.

In attempting to relate the model results to the behaviour of oceanic eddies, a key parameter to evaluate (see, for example, Kamenkovich et al., 1996) is:

$$\Pi = U_{az}^*/\beta^*(L^*)^2, \tag{13}$$

where U_{az}^* is a typical (dimensional) azimuthal velocity within the vortex and L^* a typical (dimensional) length scale of the vortex. For the present study, in which the values of the (dimensionless) parameters $\beta = 0.3$ and $\Gamma = 4.0$ are kept constant, the quantity Π can be easily expressed in terms of β and Γ. The circulation $\Gamma = \iint \omega \, dA = \oint v \cdot ds$ of the vortex can be estimated as $\Gamma^* \approx U_{az}^*(\pi L^*)$. With $\Gamma^* = \Gamma(L^*)^2/T_0$ from the scaling (see above), it follows that $U_{az}^* \approx \Gamma L^*/\pi T_0$. Inserting this and Eq. (11) in Eq. (13) gives for the model simulations presented below:

$$\Pi \approx \Gamma/\beta\pi = 4.24. \tag{14}$$

Such a value compares favourably with the value $\Pi = 2.5$ computed for the Agulhas eddy (Kamencovich et al., 1996), indicating that the model parameter range matches well with the oceanic eddy equivalent in this respect. Using for L^* a typical meddy scale at $\phi_0 = 15°N$, as above, the typical azimuthal velocity for the vortex is $U^*_{az} \approx 0.94$ m s^{-1}.

3.2. A seamount at the equator and to the south, respectively

Fig. 1 shows the trajectories of the monopole when $f_0 = 0$ and $f_0 = -5$ for four different sizes of the seamount, as well as the monopole's trajectory in the absence of any topography. The grey circles in these graphs indicate outer limits of the mountains; dark grey shading is used for $R = 0.5$ and $R = 1.5$, light grey for $R = 1.0$ and $R = 2.0$.

If the seamount is located at the equator ($f_0 = 0$), it clearly disturbs the monopole's trajectory somewhat, but the overall motion is quite similar for all R cases shown. In all four cases, the monopole actually crosses over the mountain, and the end point (at $T = 50$) is roughly the same as for the no-topography case.

For an encounter taking place far to the south ($f_0 = -5$, which means that the equator is at $y_{eq} = +50/3 \approx +13.3$), there is a clear distinction in the way the monopole moves for $R \leq 1.0$ and $R \geq 1.5$. Large seamounts (i.e. those larger in horizontal extent than the monopole) appear to rebound the monopole before it has reached the foot of the topography, similar to the rebound of a monopole encountering a north–south ridge far to the south (Van Geffen and Davies, 1999b). Even for $R = 1.0$
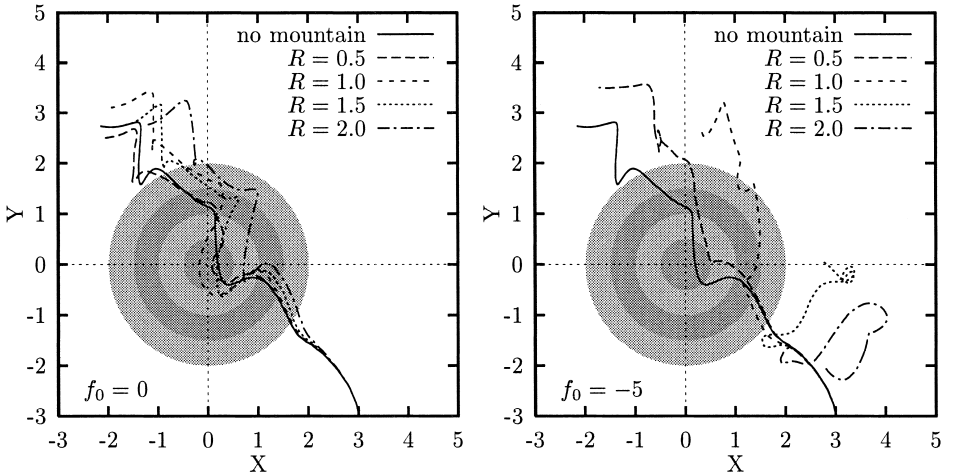

Fig. 1. Trajectory of the tracer at the maximum of vorticity of a Bessel monopole, initially at $(+3, -3)$, that encounters a seamount centred at the origin. The encounter takes place at the equator ($f_0 = 0$, left panel) and far to the south ($f_0 = -5$, right panel; the equator is at $y_{eq} = +50/3$). The seamount, given by Eq. (7), comes in four sizes and it is indicated by the shaded areas; the edges of these grey areas thus show the edges of the respective mountains. The solid line is the monopole's trajectory in the absence of any topography. All runs ended at $T = 50$. In this and all subsequent plots, only a part of the full computational domain is shown for clarity.
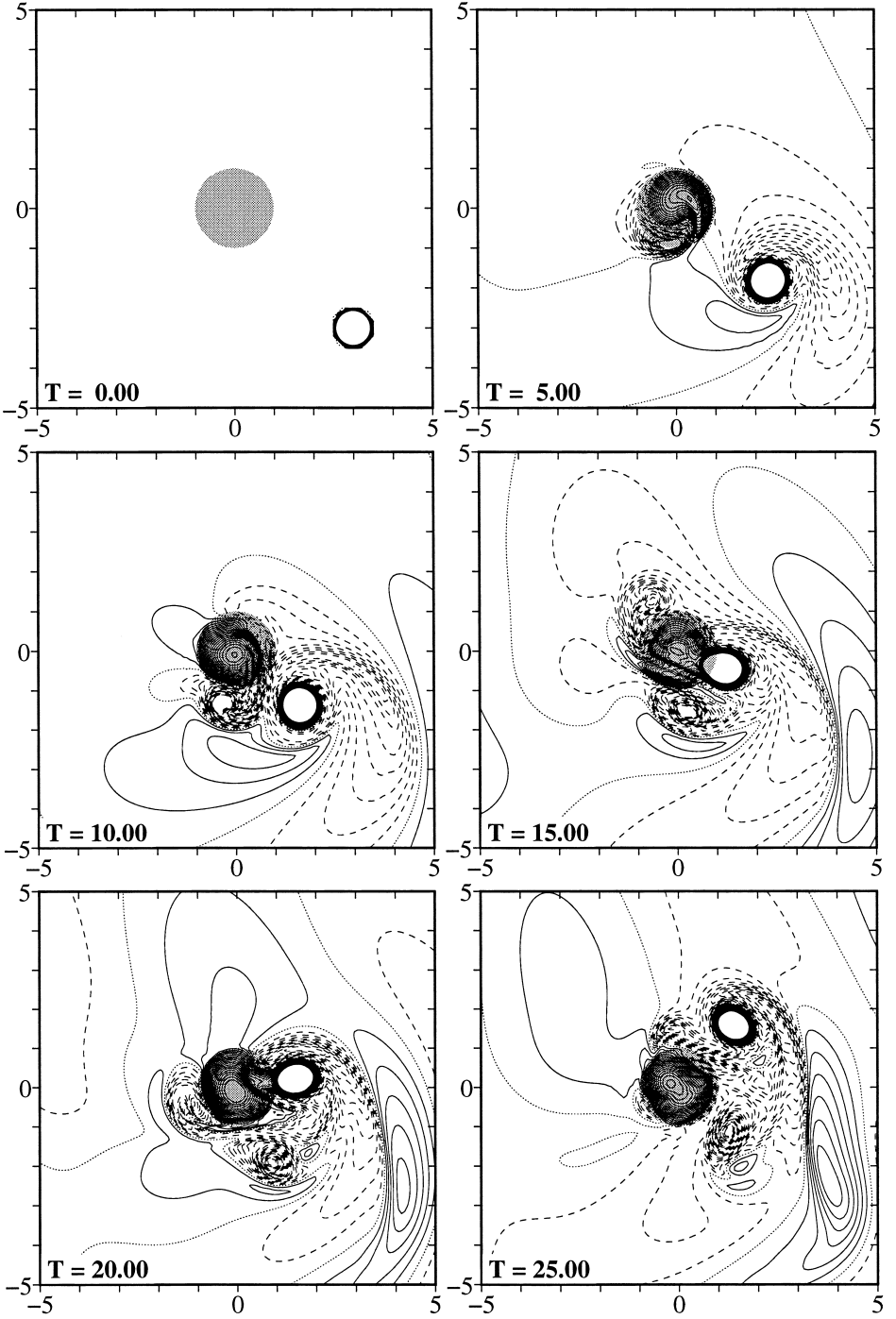
the monopole does not really reach the foot of the seamount, but the deflection is not so strong that the monopole is pushed back to the southeast: the monopole manages to deflect around the topography (which is, of course, impossible for the north–south ridge used by Van Geffen and Davies). For $R = 0.5$ the tracer at ω_{max} just reaches the foot of the seamount, before the monopole travels around the mountain to the north.

The reason for this strong topographic effect becomes clear if the relative vorticity is plotted, as in Fig. 2 for $R = 1.0$ and $f_0 = -5$: strong relative vorticity is generated at and near the mountain from the very beginning. This process is similar to the generation of relative vorticity at and behind a topographic feature in response to a flow over it (as observed by, e.g., Verron and Le Provost, 1985), where in this case the flow over the topography is generated by the monopole, not externally. The effect can be understood from the vorticity Eq. (1) if it is written in terms of potential vorticity ω_p:

$$\frac{\mathrm{D}}{\mathrm{D}t}\left(\frac{\omega + f}{H}\right) = \nu\nabla^2\omega, \tag{15}$$

where $\mathrm{D}/\mathrm{D}t$ is the material derivative. This equation says that, if viscous effects are neglected for a moment, there is conservation of potential vorticity. Fluid approaching the topography has no relative vorticity ($\omega = 0$ outside the vortex). When this fluid goes up-hill H decreases. With $f = f_0 + \beta y$ more or less constant across the topography, conservation of potential vorticity then implies that the fluid gains positive relative vorticity, which is anti-cyclonic in the southern hemisphere where the encounter is taking place. Fluid initially atop the topography also has $\omega = 0$ and when it descends it acquires negative (cyclonic) vorticity. This can clearly be seen in the second panel ($T = 5$) of Fig. 2. The motion of the fluid across the seamount finds its origin in the counter-clockwise (anti-cyclonic) motion of fluid around the monopole. The generation of relative vorticity is stronger for larger $|f_0|$; for $f_0 = 0$ there is almost no generation of relative vorticity at and near the seamount, as can be seen in Fig. 3.

Conservation of potential vorticity also means that when the positive vortex climbs the topography, it becomes weaker and ω_{max} increases again when the vortex moves down-hill if $(\omega_{max} + f) > 0$. In all cases discussed here, this is true, since $\omega_{max}(t = 0) \approx 11.8$ and $|f_0| \leq 5$, i.e. the vorticity at the centre of the vortex is relatively high compared with $|f|$. Conservation of mass of the fluid in the vortex means that when the vortex climbs the topography it becomes wider, and when it subsequently descends the topography it becomes narrower again. See Van Geffen and Davies (1999a; b) for some examples of this effect.

The time series in Fig. 2 shows clearly why the monopole is rebounded by the topography: the positive vorticity on the seamount is so strong that it prevents the monopole from climbing the topography, instead deflecting it to the north ($T = 15$–20), since the flow generated by this topography-induced vorticity is anti-cyclonic. Once the

Fig. 2. Contours of relative vorticity on the x, y-plane of a Bessel monopole, initially at $(+3, -3)$, that encounters a seamount of radius $R = 1.0$ (shaded area) with $f_0 = -5$; the equator is at $y_{eq} = +50/3$. The monopole's trajectory is given by the short-dashed line in Fig. 1 (right). Contours are drawn at intervals of 0.1 in the range $[-2.0; 2.0]$; positive contours are solid, negative dashed, and the zero contour is dotted.
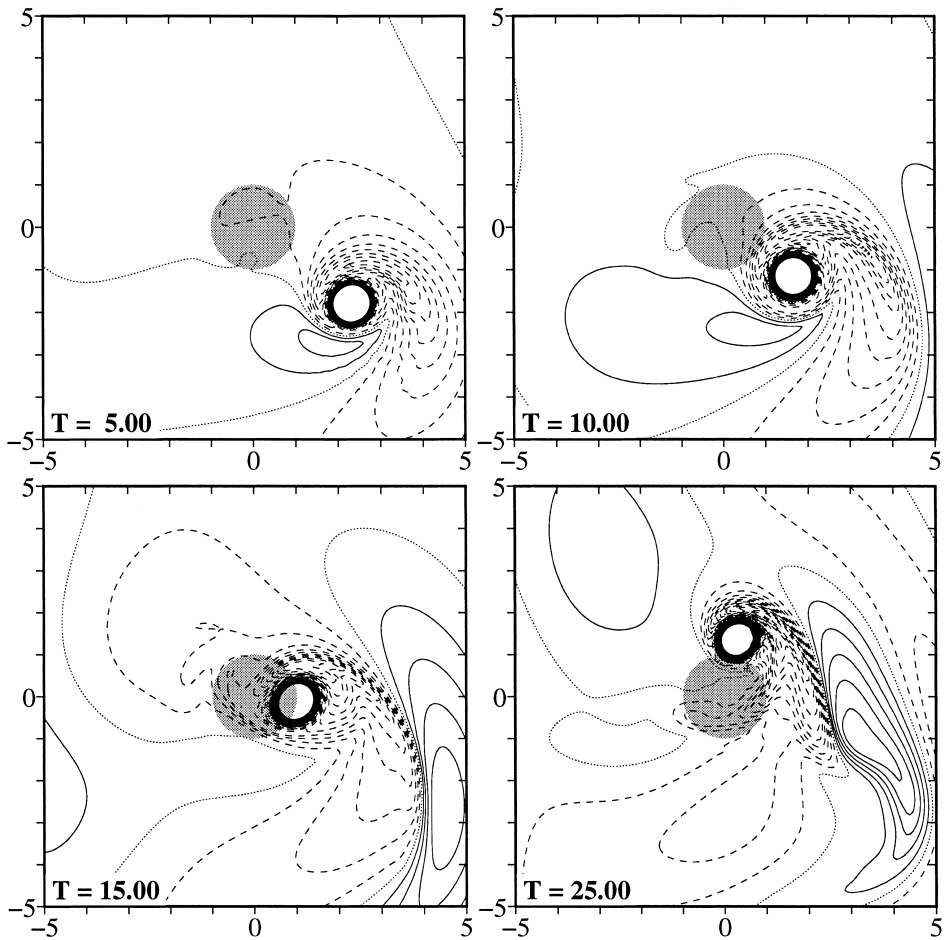
Fig. 3. Contours of relative vorticity as in Fig. 2 but for $f_0 = 0$, i.e. for a seamount at the equator ($y_{eq} = 0$). The monopole's trajectory is given by the short-dashed line in Fig. 1 (left).

monopole is free from the topographic influence, it can continue its β-induced motion to the northwest, affected of course by the vorticity in the Rossby waves and the topography-related vorticity.

The anti-cyclonic motion induced by the vorticity at the seamount moves the negative vorticity generated southwest of the mountain ($T = 5$ in Fig. 2) to the east. In the last panel of Fig. 2 ($T = 25$), this patch of negative vorticity is free from the topography and has some positive vorticity south of it. This positive patch strengthens in the subsequent evolution (not shown) and together with the negative patch forms a dipolar structure that moves south of the topography to the west.

For seamounts larger in lateral size, the topography-induced positive vorticity is stronger and makes the negative patch move around the seamount faster. This negative patch reaches the monopole before the latter has had time to travel to the north and the

pair forms a dipolar structure that moves away from the mountain, as can be seen in Fig. 4 for some stages in the evolution of the monopole for $R = 2.0$ and $f_0 = -5$. Between about $T = 10$ and $T = 20$, the monopole performs as part of that dipolar structure a loop back to the southeast, then travels to the northeast (see Fig. 1). The dipolar structure is not permanent: it falls apart and the negative patch goes to the southwest. The monopole appears not to be able to resume its northwestward β-induced motion because of the dominant influence of the ambient vorticity. Indeed, the monopole travels south again, reaching at $T = 50$ a location close to where it started (Fig. 1). The topography is a clear barrier to the monopole and the monopole is not deflected around it, as was the case of the $R \leq 1.0$ mountains. For a seamount of $R = 1.5$ the process is similar to that of $R = 2.0$, but the monopole manages to go more to the north than for $R = 2.0$, as Fig. 1
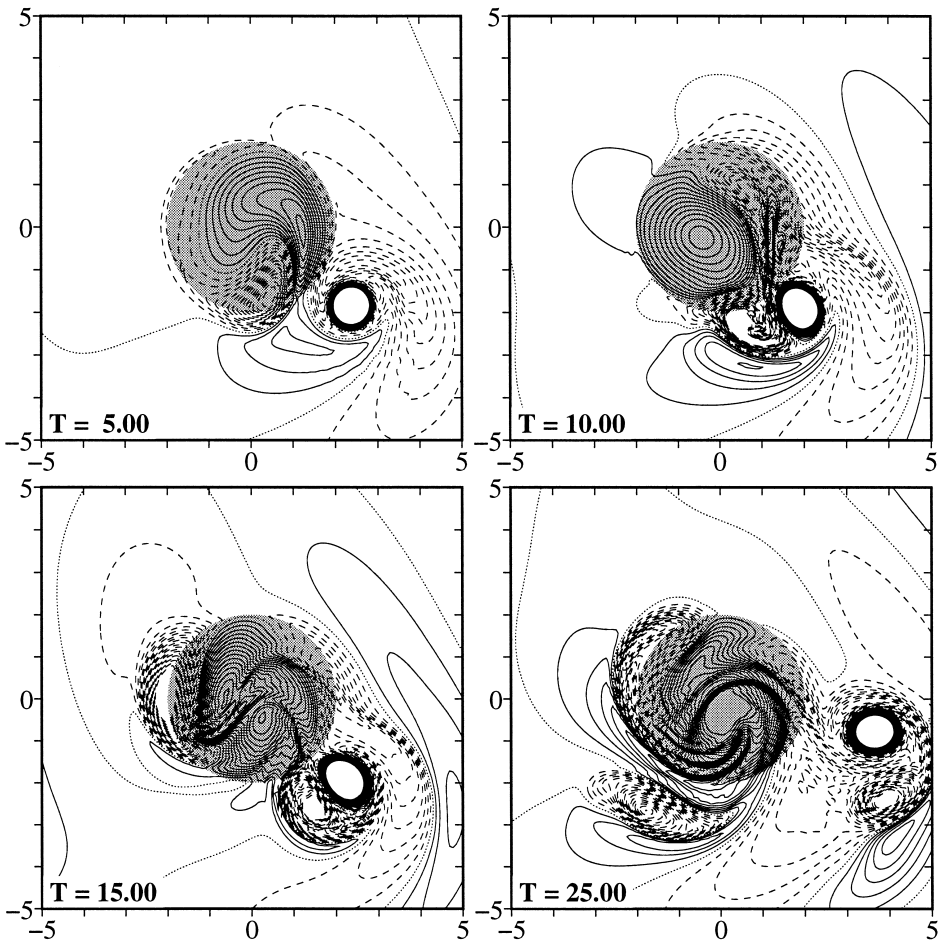

Fig. 4. Contours of relative vorticity as in Fig. 2 but for a seamount of radius $R = 2.0$. The monopole's trajectory is given by the dash-dotted line in Fig. 1 (right).

shows. The reason is that the topography-induced negative vorticity is less strong and the dipolar structure formed breaks up earlier for $R = 1.5$.

The trajectories of the monopole for f_0 between 0 and -5 are plotted in Fig. 5 for the four seamounts separately, for otherwise-identical conditions. These graphs show that the more negative f_0 is, the larger is the disturbance of the monopole's trajectory, especially for large seamounts. A mountain with $R = 2.0$, which is about four times the size of the monopole (the monopole grows somewhat in size as it evolves due to viscous effects), effectively blocks the monopole even for moderately negative f_0. A somewhat smaller seamount ($R = 1.5$) initially blocks the monopole at strong $f_0 < 0$, but the
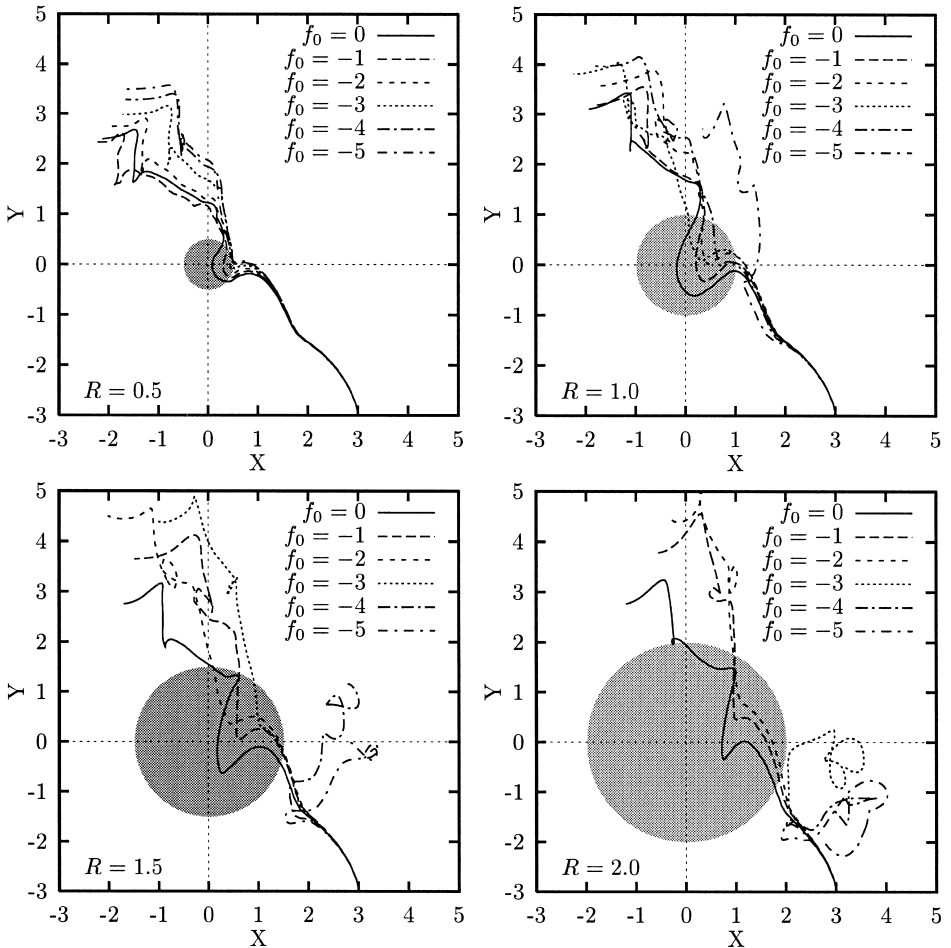
Fig. 5. Trajectory of the tracer at the maximum of vorticity of a Bessel monopole, initially at $(+3, -3)$, that encounters a seamount centred at the origin. The seamount, indicated by the shaded areas, comes in four sizes. The encounter takes place at the equator ($f_0 = 0$) or to the south ($f_0 < 0$); the trajectories for $f_0 = 0$ and $f_0 = -5$ can also be seen in Fig. 1. All runs ended at $T = 50$.

monopole is able to move around the mountain eventually (after $T = 50$, not shown). In both large seamounts, the influence of the topography on the monopole's trajectory is notable, even for low $f_0 < 0$. Smaller seamounts, up to twice the size of the monopole, also disturb the monopole's trajectory, but considerably less and the end points at $T = 50$ lie close together, with the exception of the case $R = 1.0$ and $f_0 = -5$, which shows that even relatively small seamounts can affect significantly the monopole's evolution if the encounter takes place far to the south of the equator.

3.3. A small seamount north of the equator

Since there is a clear distinction between the effect on the monopole's evolution of a small ($R \leq 1.0$; this section) and large ($R \geq 1.5$; Section 3.4) seamounts in the northern hemisphere, the discussion of these cases is split in two parts.

Fig. 6 shows for the small seamounts the trajectories for f_0 between 0 and $+5$. In all these cases, the monopole climbs the topography, moves southwest of the top and leaves the seamount again without significant deformation. For the smallest seamount ($R = 0.5$) considered here the encounter leads to only a small difference in the end points ($T = 50$) for all f_0-values.

For $R = 1.0$, there is a notable difference between low and high f_0-values. For the lowest f_0-values the trajectories are quite similar, though the monopole makes a wider turn around the top of the mountain for larger f_0. If the seamount is located further to the north, with $f_0 = +2$ or $f_0 = +3$, then the monopole is deflected more by the vorticity generated at the seamount: the monopole moves along the south-side and is free from the topography again at the (south)west side, after which it resumes its β-induced motion to the northwest; the end point is in these cases located further to the west than expected.
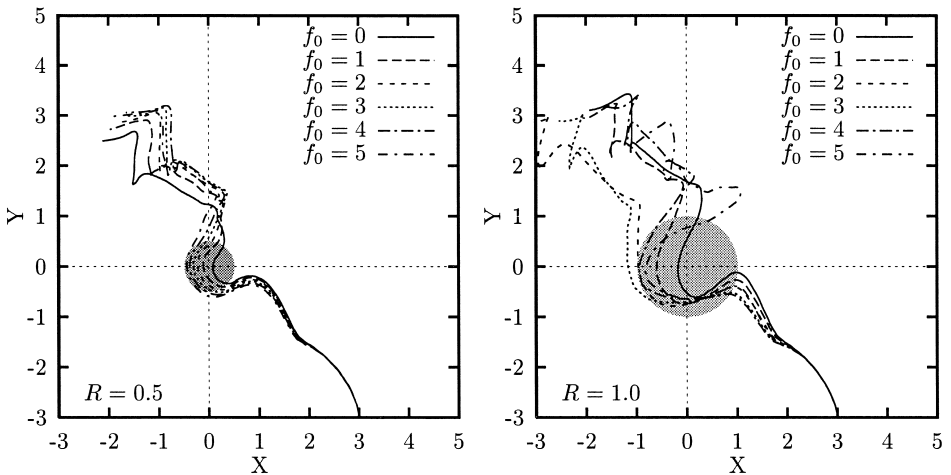

Fig. 6. Trajectories of the tracer at the maximum of vorticity as in Fig. 5 but for the two small seamounts at the equator ($f_0 = 0$) and to the north ($f_0 > 0$). All runs ended at $T = 50$; for $f_0 = +2$ at $R = 1.0$ (right graph) the end point lies just outside the left border at $x = -3.16$.

Since f_0 is positive in these cases, conservation of potential vorticity implies that the flow across the topography (caused by the monopole's rotation and motion) results in negative vorticity being generated above it and positive vorticity behind it. This is the reverse of what is seen in Fig. 2, but since the motion is now in the northern hemisphere, the vorticity of the fluid above the topography is also anti-cyclonic in sense. This motion forces the monopole to go more to the south of the top of the seamount. For a mountain far to the north ($f_0 = +4$ and $f_0 = +5$), the anti-cyclonic motion appears to be so strong that the monopole is dragged further around the top than for lower f_0-values, before it manages to move freely again. The monopole's direction of motion caused by the ambient vorticity is then first northeast, before going to the northwest again. Fig. 7 shows as an example a time sequence of vorticity plots of the $f_0 = +5$ case.

3.4. A large seamount north of the equator

The simulations discussed in Section 3.2 showed that in the southern hemisphere, the large-scale seamounts ($R \geq 1.5$) affect the monopole's evolution more than their relatively small counterparts ($R \leq 1.0$). This is also the case if the seamounts are in the northern hemisphere, but the resulting evolution is quite different from the southern-hemisphere cases. In the southern hemisphere, the monopole is seen to rebound from the topography in some cases, after which the monopole is either deflected around or completely blocked by the topographic barrier (see Fig. 5). In contrast, in the northern hemisphere the monopole can be permanently or temporarily trapped on the seamount, as is shown below. Because of this aspect of the influence of a seamount on the monopole, all northern-hemisphere runs discussed in this section, i.e. those for the seamounts with $R \geq 1.5$, are continued until $T = 100$ to determine the fate of the monopole.

At first, the motion of the monopole is as in Fig. 6 (which is for $R \leq 1.0$) and the vortex reaches the foot of the topography at the (east–)southeast side. The monopole then climbs the seamount and turns to the west, to pass south of the top, as in Fig. 6 for the small seamounts. What happens next depends very much on the value of f_0 in combination with the horizontal dimension of the seamount.

Consider first a mountain with $R = 1.5$. The monopole's trajectory for $f_0 = 0$ is shown by a solid line in Fig. 5, in which case ω_{max} stays east of the top of the topography. For $f_0 = +1$ the monopole makes a big loop around the top to the north, after which it performs two small loops, before leaving the seamount, as can be seen in Fig. 8. The subsequent motion is complicated and shows some small loops and bends, caused by the interaction with the topography-induced vorticity, but the overall motion of the monopole is to the northwest. For $f_0 = +2$ (see Fig. 8), the trajectory is similar, though with a wider loop around the top of the seamount and some small loops near the foot at the northern side. The subsequent motion to the northwest is less clear than for $f_0 = +1$ and it shows more small loops and bends, because the ambient vorticity field is stronger.

Fig. 7. Contours of relative vorticity as in Fig. 2 but for $f_0 = +5$, i.e. for a seamount far to the north (the equator is at $y_{eq} = -50/3$). The monopole's trajectory is given by the short-dash-dotted line in Fig. 6 (right).
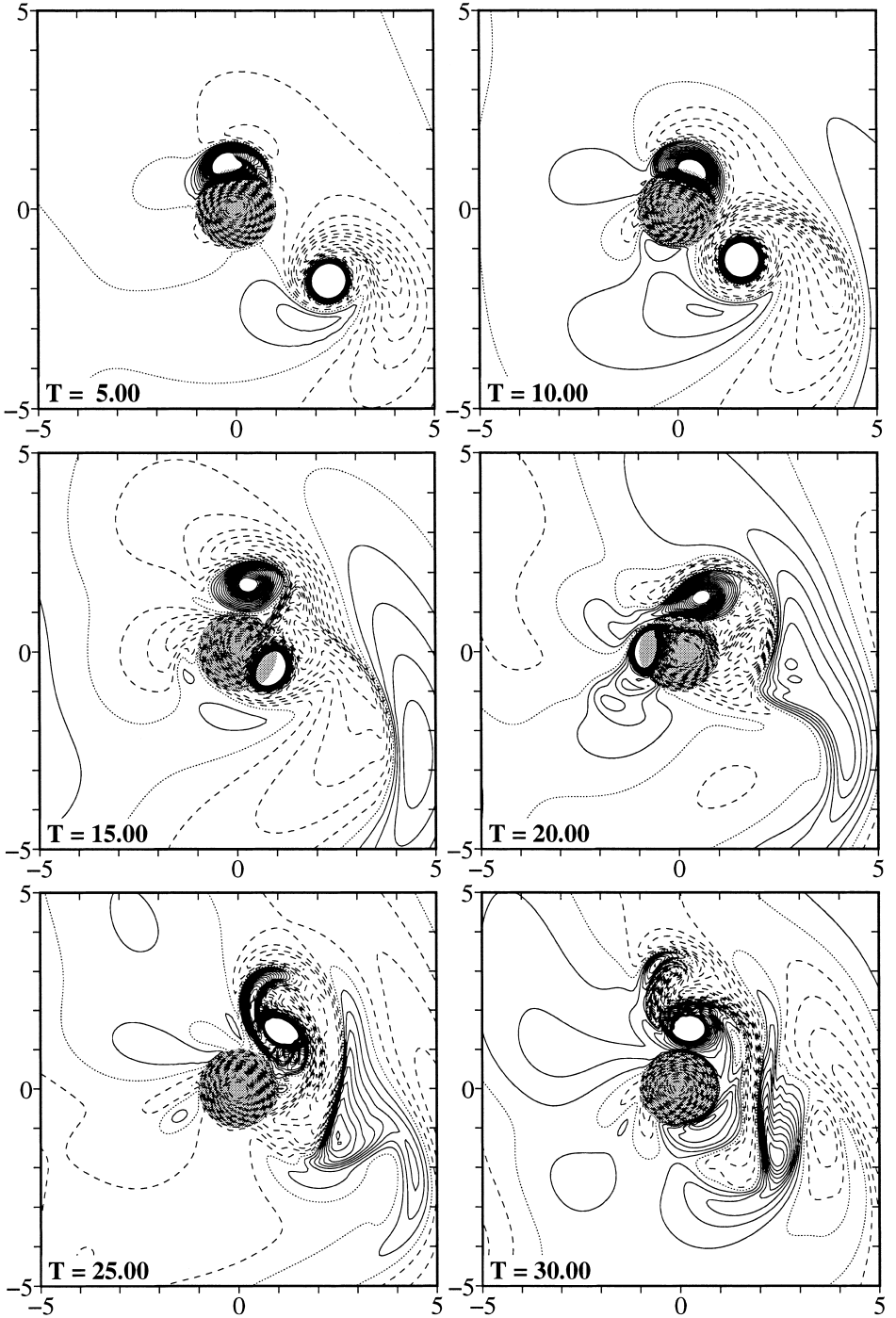
Fig. 8 also shows the trajectory for $f_0 = +5$, i.e. with the seamount located very far to the north. In this case, the monopole is deflected considerably by the topography-induced vorticity and it leaves the seamount quite quickly, without significant penetration into the zone above the seamount itself. The monopole subsequently moves in a northwest direction, until about $T = 40$. It then makes a rather sharp turn to the east, as a result of the interaction with the ambient vorticity field. At this point, the vortex is deformed considerably and after $T = 45.5$ the maximum of vorticity is no longer located at the centre of the (still clearly existing) vortex, but elsewhere in the domain. The vortex remains coherent, restores its circular form and continues its β-induced motion to the northwest. (For $f_0 = +1$, ω_{max} is at the vortex centre until $T = 81.2$ and for $f_0 = +2$ until $T = 97.9$.)

What happens for the intermediate f_0-values is quite different from these cases. For $f_0 = +3$, the monopole is trapped above the topography, as the trajectory plotted in Fig. 8 shows: the monopole circles first three times around the top of the seamount and then follows a path around the top with several small loops and bends. A similar trajectory is followed for $f_0 = +4$, except that in this case, the monopole eventually detaches from the seamount and moves freely again. To show the looping motion of the vortex more clearly, Fig. 9 shows its trajectory with time plotted vertically.

The peak in the trajectory in $f_0 = +3$ in Fig. 8, just north of the topography, at about $T = 80$, is not a sharp turn in the monopole's path, but a result of the projection of a small loop made by the monopole. Shortly after this, ω_{max} is no longer located at the centre of the vortex and somewhat later the vortex has become indistinguishable from the ambient vorticity. For $f_0 = +4$ (Fig. 9), the vortex almost undergoes the same fate: after $T = 65.6$, ω_{max} is away from the tracer location and the vortex is difficult to recognise. But the structure of the vortex is restored again and ω_{max} is (roughly) back at
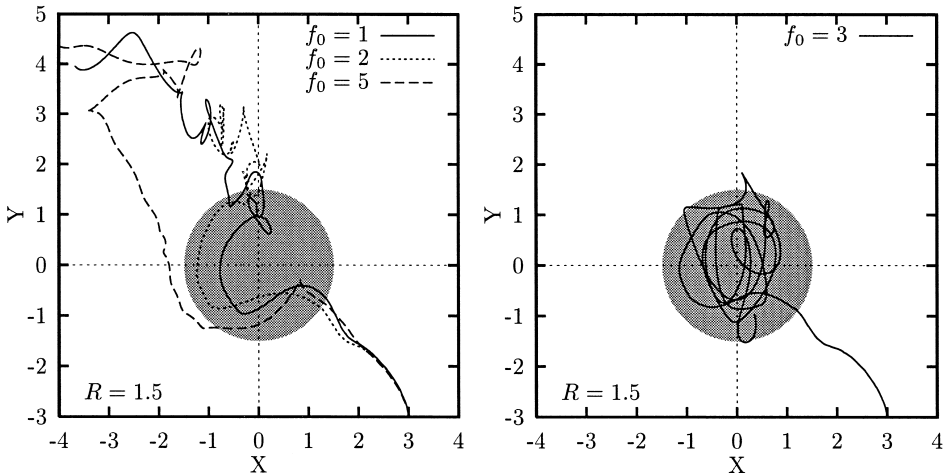

Fig. 8. Trajectories of the tracer initially at the maximum of vorticity as in Fig. 5 but for the $R = 1.5$ seamount north of the equator, for selected f_0-values. All runs ended at $T = 100$; for $f_0 = +5$ (left graph) the end point lies just outside the left border at $x = -4.5$. (The $f_0 = 0$ case is plotted in Fig. 5 until $T = 50$.)
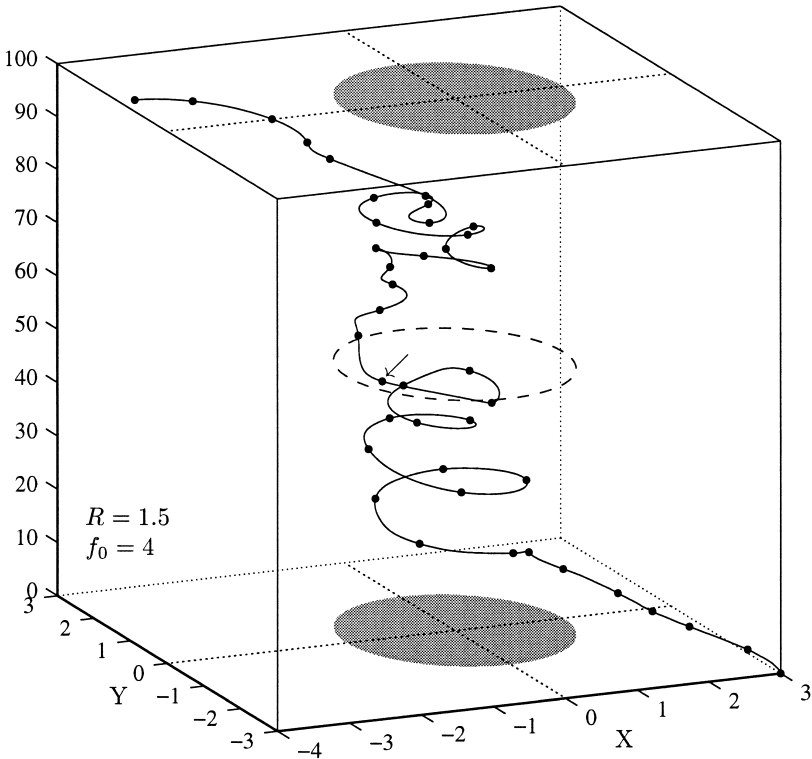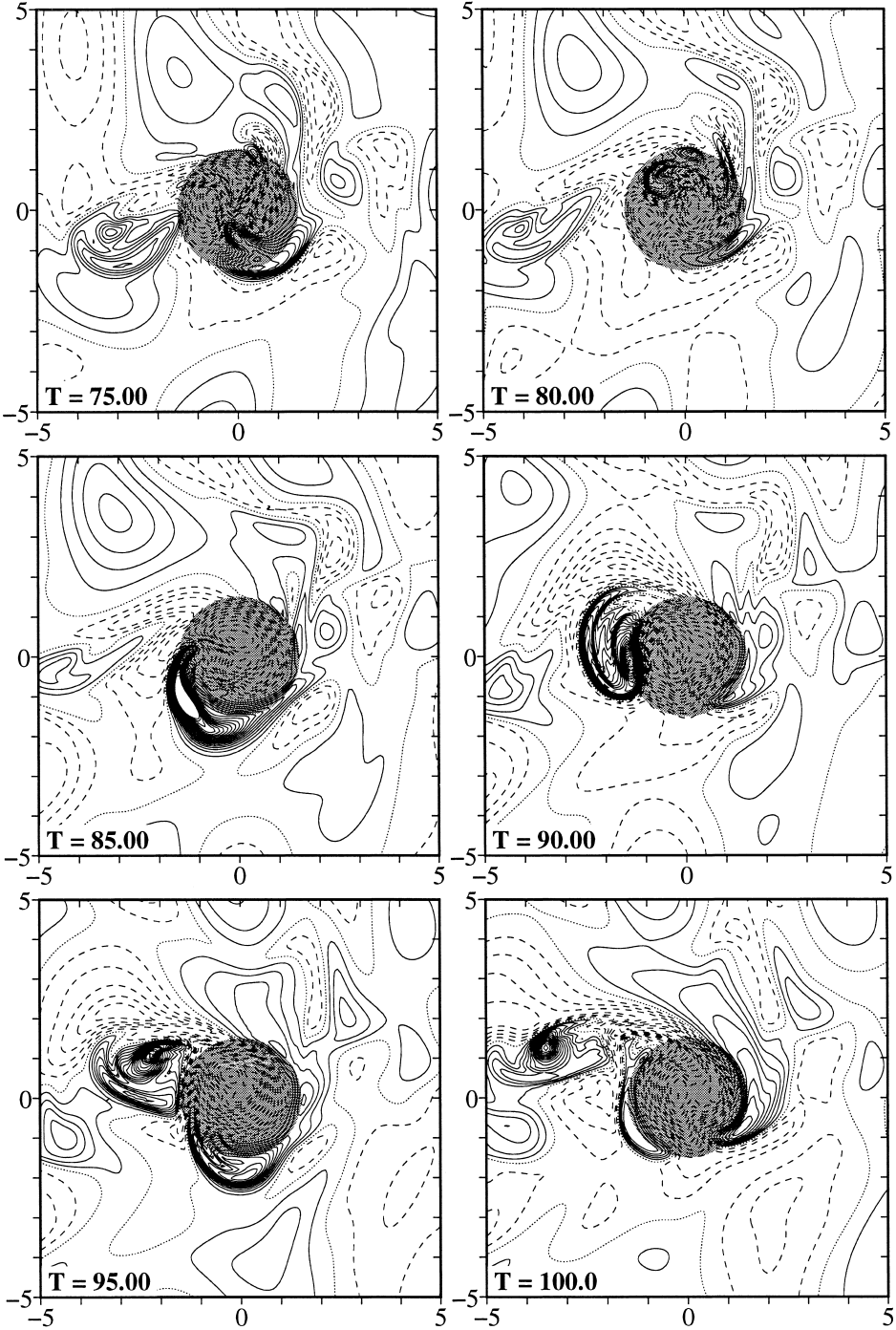
Fig. 9. Trajectory of the tracer initially at the maximum of vorticity of a Bessel monopole that encounters a seamount of $R = 1.5$ centred at the origin, with $f_0 = +4$. Time is plotted vertically and black dots are placed along the trajectory at intervals of $\Delta T = 2.5$; the run ended at $T = 100$. The grey areas at the top and bottom plane indicate the location of the topography and so does the dashed circle at $T = 50$. The arrow points to the black dot of $T = 50$.

the tracer location after $T = 82.3$, followed by a motion away from the topography. Fig. 10 shows vorticity contours of the last stages in the evolution of this case.

When the monopole encounters a seamount having $R = 2.0$, the trajectories of the tracer initially placed on the monopole (plotted in Fig. 11) are similar to those for the $R = 1.5$ counterpart case. But there are some notable differences, depending on the f_0-value.

For $f_0 = +1$ at $R = 2.0$ (Fig. 11), the monopole performs a few loops above the seamount before leaving it at the north side, followed by a motion to the northwest with several small loops, as for $f_0 = +2$ at $R = 1.5$ (Fig. 8). In both these cases, the vortex retains its structure throughout the run, without severe deformations. That is also the case for $f_0 = +2$ at $R = 2.0$ (Fig. 11), where the monopole is trapped for some time above the topography, but eventually (at about $T = 90$), it leaves the seamount; the tracer and ω_{max} are at the same point throughout the evolution.

For $f_0 = +3$ at $R = 2.0$ (Fig. 11), the monopole is trapped on the topography, as it is for the same f_0-value at $R = 1.5$ (Fig. 8). The deformations of the vortex are at $R = 2.0$
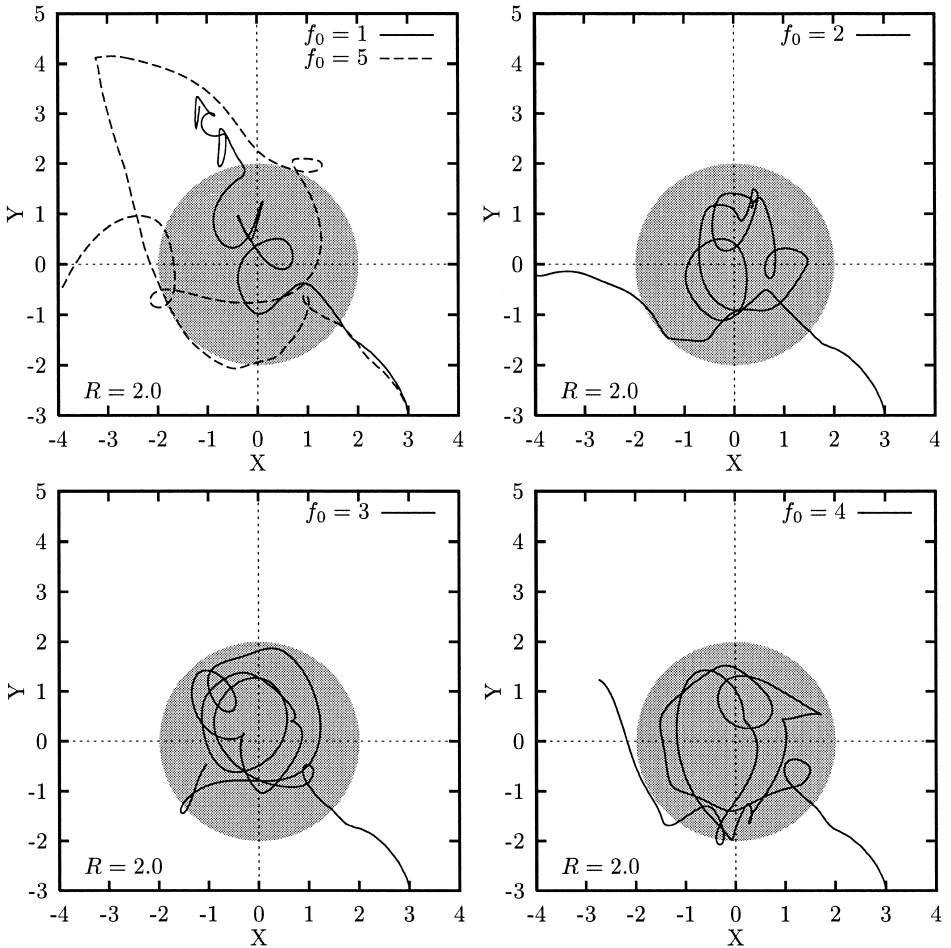
Fig. 11. Trajectories of the tracer initially at the maximum of vorticity as in Fig. 5 but for the $R = 2.0$ seamount north of the equator. All runs ended at $T = 100$; for $f_0 = +2$ and $f_0 = +5$ the end point lies just outside the left border at $x = -4.1$ and $x = -4.2$, respectively. (The $f_0 = 0$ case is plotted in Fig. 5 until $T = 50$.)

somewhat stronger and ω_{max} leaves the tracer position a little earlier than for the $R = 1.5$ case. Both large seamounts also give similar trajectories for $f_0 = +4$, but the deformations are clearly larger on the larger topographic feature. But there is a big difference. At $R = 1.5$, the vortex restores its structure (and ω_{max} returns to the tracer position) and eventually the monopole leaves the topography (see Fig. 10). At $R = 2.0$, on the other hand, the deformations are too strong and the vortex disintegrates above the

Fig. 10. Contours of relative vorticity as in Fig. 2 but for $R = 1.5$ and $f_0 = +4$ (i.e. the equator is at $y_{eq} = -40/3$). The monopole's trajectory is given in Fig. 9.

Table 1
Summary of the fate of a Bessel monopole that encounters a seamount of radius $R \geq 1.5$ at the northern hemisphere ($f > 0$), as discussed in Section 3.4

f_0	Fate at $R = 1.5$	Fate at $R = 2.0$
$+1$	crosses	crosses after few loops
$+2$	crosses	trapped → leaves after all
$+3$	trapped → destroyed	trapped → destroyed
$+4$	trapped → leaves after all	trapped → destroyed
$+5$	crosses	crosses, returns → destroyed

topography. The tracer is then simply displaced by the ambient vorticity and moves away from the topography after about $T = 93$.

For $f_0 = +5$, the trajectories at $R = 1.5$ (Fig. 8) and $R = 2.0$ (Fig. 11) are initially similar: the monopole cannot climb the topographic barrier and is deflected around the south side and thereafter travels to the northwest. Subsequently, the vortex makes a rather sharp turn to the east (at $R = 2.0$ this occurs at about $T = 35$), at which point the deformation of the vortex becomes so strong that ω_{max} moves away from the tracer location. The still-visible vortex at $R = 1.5$ then travels again to the northwest (Fig. 8). But at $R = 2.0$, the vortex turns to the southeast and encounters the topography again at about $T = 50$. As a result of the topographic influence it performs a few small loops and begins to climb the seamount. In that process, the deformations are too strong for the vortex and it disintegrates. The tracer is then simply displaced by the ambient vorticity field and is eventually found west of the mountain.

Table 1 summarises and classifies the results for the two large seamounts in the northern hemisphere in terms of the fate of the monopole as it encounters the topography.

4. Concluding remarks

In order to simulate the encounter of a class of oceanic eddies with isolated seamount-like topographic features, a 2D numerical model has been utilised to determine the possible outcome of such encounters for an incident monopolar vortex and a circularly symmetric seamount. The investigation has considered specifically the influence of (i) the north–south location where the encounter takes place, and (ii) the horizontal scale of the topography, for otherwise-identical conditions.

The monopole, with initial radius $a = 0.5$ (it grows somewhat due to viscous effects as time goes on) has positive vorticity — i.e. it is cyclonic (anti-cyclonic) in sense in the northern (southern) hemisphere. This vortex moves to the northwest as a result of the β-effect, where it encounters an isolated, cosine-shaped, axisymmetric topographic feature, representing a seamount, with a maximum height of $h_{max} = 0.4$ (relative to the default fluid depth $H = 1$) and a radius R varying between $R = a = 0.5$ and $R = 4a = 2.0$. This seamount is located somewhere between far south ($f_0 = -5$) and far north ($f_0 = +5$) of the equator, the equator being located at $y_{eq} = -f_0/\beta$; for this study

$\beta = 0.3$ and f_0 is varied. If the monopole is to model a real-life vortex in the Earth's ocean with a diameter of, say, 10^5 m then the scaling is such that $f_0 = +5$ represents roughly a latitude of 15°N with $y_{eq} \approx -17$ (Section 3.1).

The results presented in the present paper show that there is a distinction in the possible outcome of the encounter depending on whether the seamount has a horizontal scale comparable with that of the vortex ($R \leq 1.0$) or larger ($R \geq 1.5$). And there is also a difference between encounters taking place in the northern ($f_0 > 0$) and southern ($f_0 < 0$) hemisphere, especially if the distance to the equator is large.

Relatively small seamounts ($R \leq 1.0$) in the southern hemisphere or at the equator (Fig. 5) affect the monopole's trajectory slightly, and the position of the vortex some time after the encounter is similar to the position the monopole would have had if no topography had been present; the difference in these positions increases for larger $|f_0|$, i.e. further south. For the larger seamounts ($R \geq 1.5$; Fig. 5), there is some difference in the monopole's trajectory if f_0 is not too strong, in which case the monopole's eventual position is further to the north than if there is no topography. If the latter is located far to the south, however, the monopole can be rebounded along its direction of approach and the seamount acts as a complete barrier to the monopole. In all the encounters taking place in the southern hemisphere or at the equator, the monopole retains its integrity, though there is some deformation of the monopole as it moves. And if the monopole passes or crosses the topography, it does so east of the top of the seamount.

For seamounts in the northern hemisphere ($f_0 > 0$) comparable in size with that of the vortex ($R \leq 1.0$), the monopole crosses the seamount to the west of the top without significant deformation (Fig. 6); the ''end point'' of the vortex' motion is roughly the same as without a seamount present. For larger seamounts ($R \geq 1.5$; Figs. 8, 9 and 11) north of the equator the encounter leads to complicated trajectories and strong deformations. At low latitudes, the monopole is deformed severely but survives the crossing and then follows a trajectory with several small loops and bends to the northwest. At higher latitudes the vortex can be trapped by the topography, with a trajectory consisting of orbits around the top, with small loops superimposed on its motion. In some cases the vortex is able subsequently to escape from the topographic trapping, while in other cases it is shown to be destroyed by the interaction with the topography-induced vorticity. For a seamount located even further to the north, the topography-induced vorticity is so strong that the monopole is deflected along the south side of the mountain to the west, with considerable deformations and a complicated trajectory. It has been shown that the monopole is also able to turn to the southeast and again encounter the topography, with subsequent disintegration of the vortex, if the topographic feature is very large (Fig. 11).

The simulations discussed in the present paper have been carried out with a positive monopole, i.e. one that has cyclonic (anti-cyclonic) vorticity in the northern (southern) hemisphere, and which travels to the northwest. For a negative monopole, which travels to the southwest, cyclonic/north and anti-cyclonic/south have to be interchanged. Hence, a negative monopole can be rebounded in the northern hemisphere and trapped on the southern hemisphere by a seamount, and there is no basic difference between positive and negative vortices. At least that is the situation in numerical simulations as those presented here; in the laboratory it is difficult to have stable negative vortices (anti-cyclones on the northern hemisphere; see Kloosterziel and Van Heijst, 1991).

The monopole used in the present study has a single signed vorticity distribution, i.e. it has a non-vanishing circulation. A so-called isolated monopole, which has a total circulation $\iint \omega \, dA$ equal to zero, with a positive (negative) core also travels to the northwest (southwest) due to the β-effect, but along a trajectory more to the north (south) than the non-isolated monopole (Carnevale et al., 1991; Van Heijst, 1994). This difference is caused by the presence of an oppositely signed ring of vorticity around the core for the vortex, part of which is shed in the form of small vortices as the monopole moves, hence the interaction with the ambient vorticity field will be different, though the basic interaction mechanism is the same (see Carnevale et al., 1991); this matter has not been investigated any further in this study.

The precise structure of the topographic feature has some influence on the outcome too, of course. The seamount used here, given by Eq. (7), has the profile of half a cosine: $h_{max}\cos(r\pi/2R)$. A topography with a less steep slope near its foot — such as a full-cosine function $h_{max}[\cos(r\pi/R) - 1]/2$ — allows the monopole to climb a little further towards the top. Near the top, however, such a topographic profile is steeper again than the half-cosine counterpart and the ''effective'' size of the full-cosine mountain is therefore somewhat smaller than that of the half-cosine of Eq. (7). Thus, the range of possible outcomes of the encounter shifts a little to larger seamount radii, but the different regimes are similar.

For a negative h_{max}, the topography is obviously a pit. If the (positive) monopole encounters the pit from the southeast, the effect of the pit on the monopole's evolution will be similar to the effect of the mountain discussed in Section 3, but with north and south of the equator interchanged: a pit in the northern hemisphere can rebound the vortex, and the monopole can be trapped by a pit in the southern hemisphere. The details of the evolution of the monopole will no doubt be somewhat different though. Fig. 12
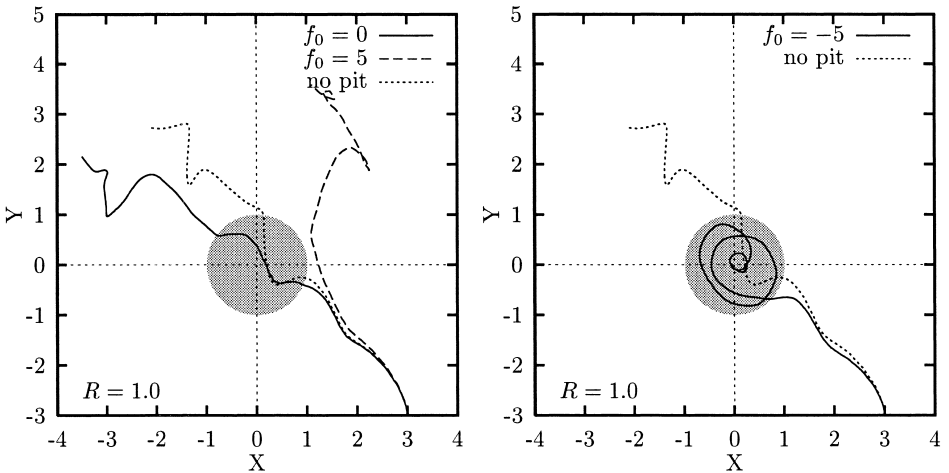

Fig. 12. Trajectories of the tracer at the maximum of vorticity of a Bessel monopole, initially at $(+3, -3)$, that encounters a pit of radius $R = 1.0$ centred at the origin (shaded region). The encounter takes place at the equator ($f_0 = 0$), in the northern hemisphere ($f_0 = +5$) and in the southern hemisphere ($f_0 = -5$). The dotted curve in both graphs shows the monopole's trajectory if there is no topography. All runs ended at $T = 50$.

shows as an example a pit with the half-cosine profile given by Eq. (7) with radius $R = 1.0$ and $h_{max} = -0.4$ at three latitudes. In the equatorial case, the monopole crosses the pit and ends up more to the west than in the case of a mountain (cf. Fig. 5). In the northern hemisphere, with $f_0 = +5$, the pit deflects the monopole in a way similar to a mountain on the southern hemisphere with $f_0 = -5$ (Fig. 5). And if the pit is in the southern hemisphere ($f_0 = -5$), it traps the monopole, unlike for the mountain of the same radius in the northern hemisphere (Fig. 6), where the monopole crosses the mountain. The reason for the latter difference is that as the monopole descends into the pit it become narrower and stronger, whereas it becomes wider and weaker as it climbs the mountain. A monopole crossing a pit is thus less susceptible to deformations than a monopole crossing a mountain under otherwise-identical conditions. The example shows that the pit topography case deserves a study of the full parametric range of values for f_0 and R, but that falls outside the scope of the present paper.

In summary, what happens to a monopolar vortex when it encounters the topographic feature depends mostly on whether the encounter takes place in the northern or southern hemisphere, and on the lateral size of the topography relative to the size of the vortex: the bigger the seamount and/or the further away from the equator, the more dramatic the influence can be on the monopole's evolution, leading to the possible destruction of the vortex.

Acknowledgements

References

Arakawa, A., 1966. Computational design for long-term numerical integration of the equations of fluid motion: two-dimensional incompressible flow. Part I. J. Comp. Phys. 1, 119–143.

Bengtsson, L., Lighthill, M.J. (Ed.), 1982. Intense Atmospheric Vortices. Springer-Verlag, Berlin.

Bograd, S.J., Rabinovich, A.B., LeBlond, P.H., Shore, J.A., 1997. Observations of seamount-attached eddies in the North Pacific. J. Geophys. Res. 102 (C6), 12441–12456.

Bower, A.S., Armi, L., Ambar, I., 1995. Direct evidence of meddy formation off the southwestern coast of Portugal. Deep-Sea Res. 42, 1621–1630.

Carnevale, G.F., Vallis, G.K., Purini, R., Briscolini, M., 1988. Propagation of barotropic modons over topography. Geophys. Astrophys. Fluid Dyn. 41, 45–101.

Carnevale, G.F., Kloosterziel, R.C., Van Heijst, G.J.F., 1991. Propagation of barotropic vortices over topography in a rotating fluid. J. Fluid Mech. 233, 119–139.

Eriksen, C.C., 1991. Observations of amplified flows atop a large seamount. J. Geophys. Res. [Oceans] 96, 15227–15236.

Gill, A.E., 1982. Atmosphere–Ocean Dynamics. Academic Press, London, UK.

Goldner, D.R., Chapman, D.C., 1997. Flow and particle motion induced above a tall seamount by steady and tidal background currents. Deep-Sea Res. 44, 719–744.

Grimshaw, R., Broutman, D., He, X., Sun, P., 1994. Analytical and numerical study of a barotropic eddy on a topographic slope. J. Phys. Oceanogr. 24, 1587–1607.

Hopfinger, E.J., Van Heijst, G.J.F., 1993. Vortices in rotating fluids. Annu. Rev. Fluid Mech. 25, 241–289.

Kamenkovich, V.M., Leonov, Y.P., Nechaev, D.A., Byrne, D.A., Gordon, A.L., 1996. On the influence of bottom topography on the Agulhas eddy. J. Phys. Oceanogr. 26, 892–912.

Kloosterziel, R.C., Van Heijst, G.J.F., 1991. An experimental study of unstable barotropic vortices in a rotating fluid. J. Fluid Mech. 223, 1–24.

Kunze, E., Sanford, T.B., 1993. Submesoscale dynamics near a seamount: Part I. Measurements of Ertel vorticity. J. Phys. Oceanogr. 23, 2567–2588.

Pedlosky, J., 1987. Geophysical Fluid Dynamics, 2nd edn. Springer-Verlag, New York, USA.

Richardson, P.L., 1993a. Tracking ocean eddies. American Scientist 81, 261–271.

Richardson, P.L., 1993b. A census of eddies observed in North Atlantic SOFAR float data. Prog. Oceanogr. 31, 1–50.

Shapiro, G.I., Meschanov, S.L., Emelianov, M.V., 1995. Mediterranean lens 'Irving' after its collision with seamounts. Oceanologica Acta 183, 309–318.

Van Geffen, J.H.G.M., Davies, P.A., 1999a. Interaction of a monopolar vortex with a topographic ridge. Geophys. Astrophys. Fluid Dyn. 90, 1–41.

Van Geffen, J.H.G.M., Davies, P.A., 1999b. A monopolar vortex encounters a north–south ridge or trough. Fluid Dyn. Res. (in press).

Van Heijst, G.J.F., 1994. Topography effects on vortices in a rotating fluid. Meccanica 29, 431–451.

Verron, J., Le Provost, C., 1985. A numerical study of quasi-geostrophic flow over isolated topography. J. Fluid Mech. 154, 231–252.